

Single-molecule tracking of tau reveals fast kiss-and-hop interaction with microtubules in living neurons

Dennis Janning^{a,*}, Maxim Igaev^{a,*}, Frederik Sündermann^a, Jörg Brühmann^a, Oliver Beutel^b, Jürgen J. Heinisch^c, Lidia Bakota^a, Jacob Piehler^b, Wolfgang Junge^d, and Roland Brandt^a

^aDepartment of Neurobiology, ^bDepartment of Biophysics, ^cDepartment of Genetics, and ^dDepartment of Biophysics, University of Osnabrück, D-49076 Osnabrück, Germany

ABSTRACT The microtubule-associated phosphoprotein tau regulates microtubule dynamics and is involved in neurodegenerative diseases collectively called tauopathies. It is generally believed that the vast majority of tau molecules decorate axonal microtubules, thereby stabilizing them. However, it is an open question how tau can regulate microtubule dynamics without impeding microtubule-dependent transport and how tau is also available for interactions other than those with microtubules. Here we address this apparent paradox by fast single-molecule tracking of tau in living neurons and Monte Carlo simulations of tau dynamics. We find that tau dwells on a single microtubule for an unexpectedly short time of ~40 ms before it hops to the next. This dwell time is 100-fold shorter than previously reported by ensemble measurements. Furthermore, we observed by quantitative imaging using fluorescence decay after photoactivation recordings of photoactivatable GFP-tagged tubulin that, despite this rapid dynamics, tau is capable of regulating the tubulin–microtubule balance. This indicates that tau’s dwell time on microtubules is sufficiently long to influence the lifetime of a tubulin subunit in a GTP cap. Our data imply a novel kiss-and-hop mechanism by which tau promotes neuronal microtubule assembly. The rapid kiss-and-hop interaction explains why tau, although binding to microtubules, does not interfere with axonal transport.

Monitoring Editor

Jennifer Lippincott-Schwartz
National Institutes of Health

Received: Jun 13, 2014

Revised: Aug 15, 2014

Accepted: Aug 20, 2014

INTRODUCTION

The cytoskeleton and its dynamic regulation are central for practically all aspects of cellular functions. In neurons, the microtubule-associated protein (MAP) tau regulates microtubule (MT) dynamics and plays a major role in neurodegenerative diseases such as Alzheimer’s disease (Ittner and Götz, 2010; Irwin *et al.*, 2013; Spillantini and Goedert, 2013). The general belief is that the vast majority of tau molecules decorate axonal MTs, thereby stabilizing them. During disease, hyperphosphorylation or aggregation of tau

supposedly causes the detachment of tau from MTs, followed by their breakdown (Selkoe, 2013).

In addition to its role in regulating microtubule dynamics, it has also become evident that tau is a multifaceted protein that interacts with various proteins and fulfills diverse functions in different neuronal compartments (Morris *et al.*, 2011). However, it is unknown how tau exerts its non–MT-related functions in the cell body or dendrites when being attached to MTs (Ittner *et al.*, 2010). It is also surprising that neither elevated nor reduced tau levels affect axonal transport processes despite tau being a potential obstacle for motor proteins (Yuan *et al.*, 2008).

To address the apparent paradox that tau regulates MT dynamics but does not interfere with MT-dependent axonal transport, we performed fast single-molecule tracking (SMT) of tau in living neuronally differentiated cells and primary neurons. The spatial resolution of SMT (~20 nm) was high enough to discriminate between tau being attached to one particular MT or to its neighbor. Step-size distribution (SSD) analysis of pseudotrajectories revealed hops of tau between neighboring MTs, indicating that tau can have multiple binding partners within a few tens of milliseconds. The results were

This article was published online ahead of print in MBoC in Press (<http://www.molbiolcell.org/cgi/doi/10.1091/mbc.E14-06-1099>) on August 27, 2014.

*These are co–first authors.

Address correspondence to: Roland Brandt (brandt@biologie.uni-osnabrueck.de). Abbreviations used: FDAP, fluorescence decay after photoactivation; MAP, microtubule-associated protein; MT, microtubule; SSD, step-size distribution; syp, synaptophysin; TIRF, total internal reflection fluorescence.

© 2014 Janning, Igaev, *et al.* This article is distributed by The American Society for Cell Biology under license from the author(s). Two months after publication it is available to the public under an Attribution–Noncommercial–Share Alike 3.0 Unported Creative Commons License (<http://creativecommons.org/licenses/by-nc-sa/3.0>).

“ASCB®,” “The American Society for Cell Biology®,” and “Molecular Biology of the Cell®” are registered trademarks of The American Society for Cell Biology.

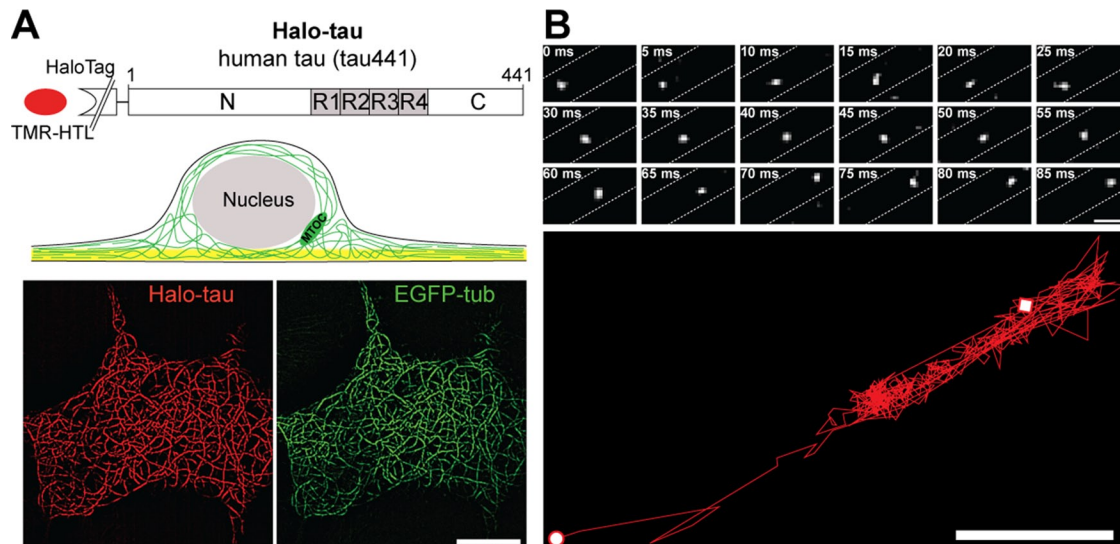


FIGURE 1: Single-molecule tracking reveals undirected fast movement of tau in processes of neural cells. (A) Schematic representation of the Halo-tagged tau fusion construct (Halo-tau) and the visualization of a thin cellular layer by TIRF microscopy. The microtubule-binding repeats (R1–R4) are indicated by the gray boxes, and the evanescent field close to the cellular attachment site is shown in yellow. Bottom, colocalization of Halo-tau (left) and monomeric enhanced GFP-tagged α -tubulin (EGFP-tub; right) as visualized by TIRF microscopy of the cell body of living PC12 cells. Sum projections of 1000 consecutive frames were recorded. Scale bar, 10 μ m. MTOC, microtubule-organizing center. (B) Time series of individual Halo-tau molecules moving in a process of a neuronally differentiated PC12 cell. Motion during the first 85 ms. Dashed lines indicate the border of the process. A trajectory generated from the complete time series (2.2 s = 440 frames) is shown below, indicating undirected fast movement both longitudinally and transversally. The starting point is indicated by a circle and the end by a square. Scale bar, 0.5 μ m.

validated by Monte Carlo simulation of tau hopping in a cellular process filled with MTs. Tau-induced changes in MT dynamics were monitored by quantitative imaging using fluorescence decay after photoactivation (FDAP) recordings of photoactivatable green fluorescent protein (PAGFP)-tagged α -tubulin.

This is the first study in which the interaction of tau with MTs in living neurons has been evaluated by direct single-molecule observations. The approach provides a novel method to follow physiological or pathological changes in the tau–MT interaction in living neurons with unprecedented precision.

RESULTS

Single tau molecules show undirected fast movement in processes of neural cells

To assess the behavior of tau in neuronal processes, single, fluorescently labeled tau molecules were tracked with a temporal resolution of 5 ms. HaloTag was fused to the amino terminus of human tau, where it does not interfere with the MT interaction that is mediated by tau's carboxy-terminal half (Gauthier-Kemper *et al.*, 2011; Figure 1A, top). The focal plane of the total internal reflection fluorescence (TIRF) microscope was adjusted to capture MTs (Figure 1A).

A diffusing tau molecule is so fast that it produces spatially blurred fluorescence that submerges in the background. In fact, a freely diffusing tau molecule would cover a distance of \sim 400 nm during 5 ms. Thus the signal intensity clearly surmounts the background only if tau is bound to a MT filament, which allows tracking subsequent MT-binding events of single tau molecules. Individual tau molecules bound to MTs could be localized with a precision of \sim 20 nm by determining the centroid of its diffraction-limited fluorescence signal. Unexpectedly, we observed tau molecules rapidly moving within some tens of milliseconds between binding sites that were several hundred nanometers apart (Figure 1B, top, and

Supplemental Movie S1). A typical trajectory of 440 frames revealed undirected, fast, longitudinal and transversal displacements of fluorescent tau in the cellular process (Figure 1B, bottom). This appears inconsistent with a previous study (Konzack *et al.*, 2007). By using fluorescence recovery after photobleaching (FRAP), the authors recorded the recovery of fluorescence in a large ensemble of tau molecules and, by fitting their data by some reaction-diffusion model, they estimated a rather long dwell time of tau on MTs, namely \sim 4 s. It was also speculated that bound tau might slowly slide on the surface of MTs (Hinrichs *et al.*, 2012). Previous treatments of FDAP/FRAP data referred to the whole MT bundle. Here, for the first time, the binding to single MT filaments is resolved in living cells. Deficiencies of the previous models and a rigorous reaction-diffusion model accounting for the bundle-structure of MT filaments, which leads to a 100-fold correction to the long apparent dwell-time, will be detailed elsewhere (Igaev *et al.*, 2014).

Tau interacts with microtubules via a kiss-and-hop mechanism in processes of neural cells

The spatial resolution of single-molecule tracking (\sim 20 nm) was high enough to discriminate between tau being attached to one particular MT or to its neighbor in processes of PC12 cells (Figure 2A). Note that the spacing between MTs in PC12 neurites is \sim 70 nm (Jacobs and Stevens, 1986), a much higher value than the typical MT–MT distance in axons (Hirokawa and Takemura, 2005) due to the fact that PC12 cells do not develop axonal compartmentalization. Figure 2B (see also Supplemental Movie S2) documents the “pseudotrajectory” of binding events of tau over time (for a real trajectory, see Figure 2C). It is also evident that tau binds to several neighboring MTs in the transversal direction during the recording time (Figure 2B).

As a control, we analyzed the behavior of synaptophysin (syp), a marker for fast axonal transport (Supplemental Movie S3). If tau

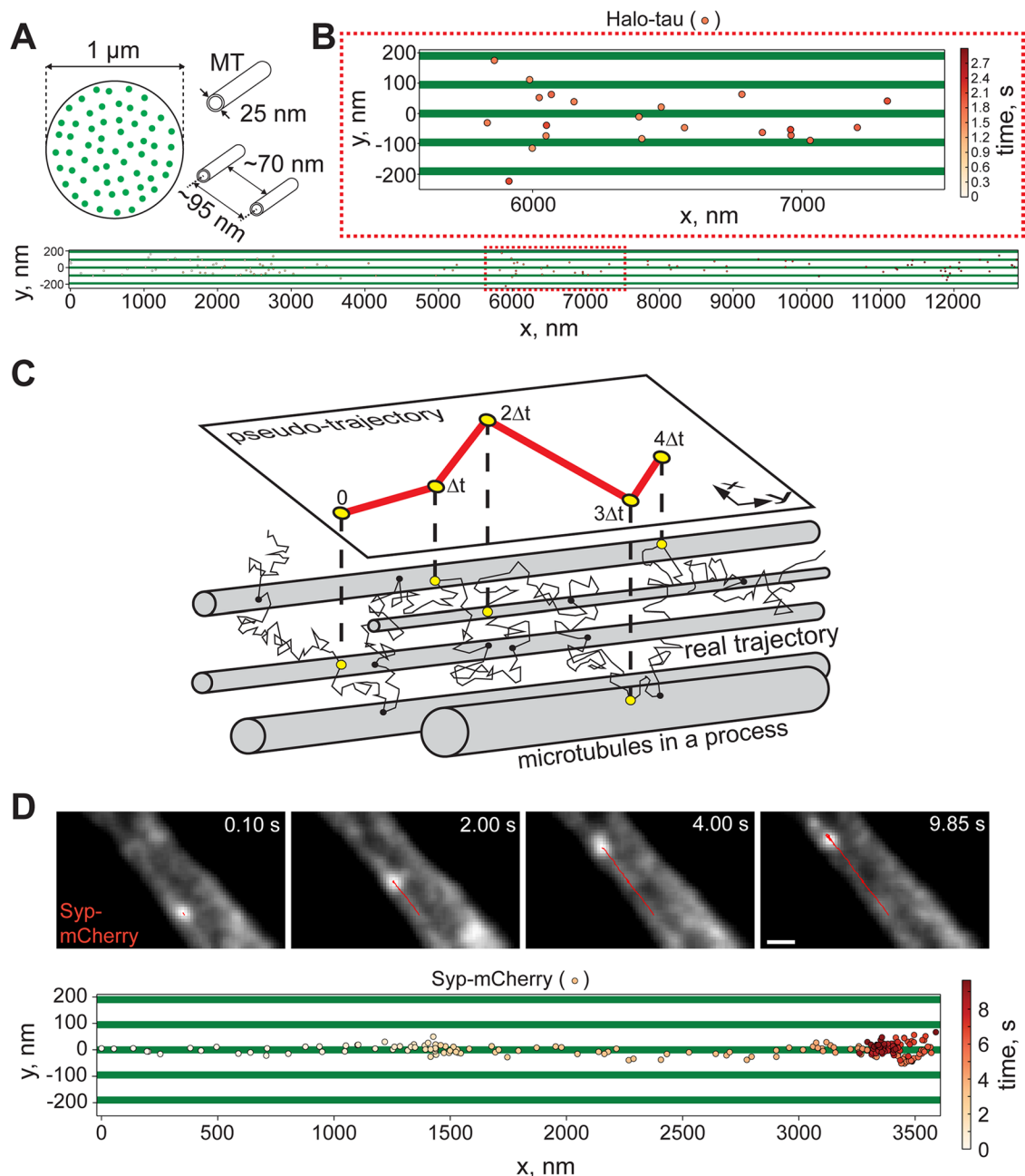


FIGURE 2: Tau interacts with multiple microtubules in processes of PC12 cells. (A) Schematic representation showing the geometry and MT distribution in a process of a neuronally differentiated PC12 cell. (B) Localization of a single Halo-tau molecule in a PC12 cell process over time (for a high-resolution version see Supplemental Figure S1). For comparison, thickness and density of MTs are schematically indicated by green bars. Top, enlargement of the indicated segment. (C) Schematic representation of a real trajectory of a molecule moving between microtubules in a bundle is shown in black. Yellow and black circles indicate binding events of tau with microtubules. The recorded pseudotrajectory is indicated in red. Only the binding events within the time frame (Δt) are detected and indicated by the yellow circles. (D) Time series showing the movement of a syp-mCherry-tagged vesicle in a PC12 cell process. In contrast to tau, localization of syp-mCherry over time indicates directional movement along a single MT. Scale bar, $1\ \mu\text{m}$.

hops between microtubules on a stationary microtubule array, we would expect that syp would not reveal transversal displacement between adjacent MTs. Indeed, a representative two-dimensional (2D) projection of binding positions of syp over time (Figure 2D, top, and Supplemental Movie S4) showed directional lateral movement on a single MT filament with small transversal spread. This behavior clearly differed from what was observed for the tau protein.

We observed fast longitudinal and transversal displacements of tau in the cellular process (Figure 1B). To characterize quantitatively

the displacements of tau, we calculated SSDs. Here the probability of a particle moving over a certain distance within a fixed time interval Δt was evaluated. Figure 3A represents an SSD histogram plotted using >1000 2D pseudotrajectories for the first time step (see *Materials and Methods*). The SSD analysis of the pseudotrajectories revealed the presence of three peaks, at ~ 95 , ~ 190 , and ~ 285 nm. Remarkably, these values correspond to the distance between the centers of neighboring MTs, reflecting hops $1 \rightarrow 2$ and multiples thereof (hops $1 \rightarrow 3$, $1 \rightarrow 4$; Figure 3A), indicating that tau can have

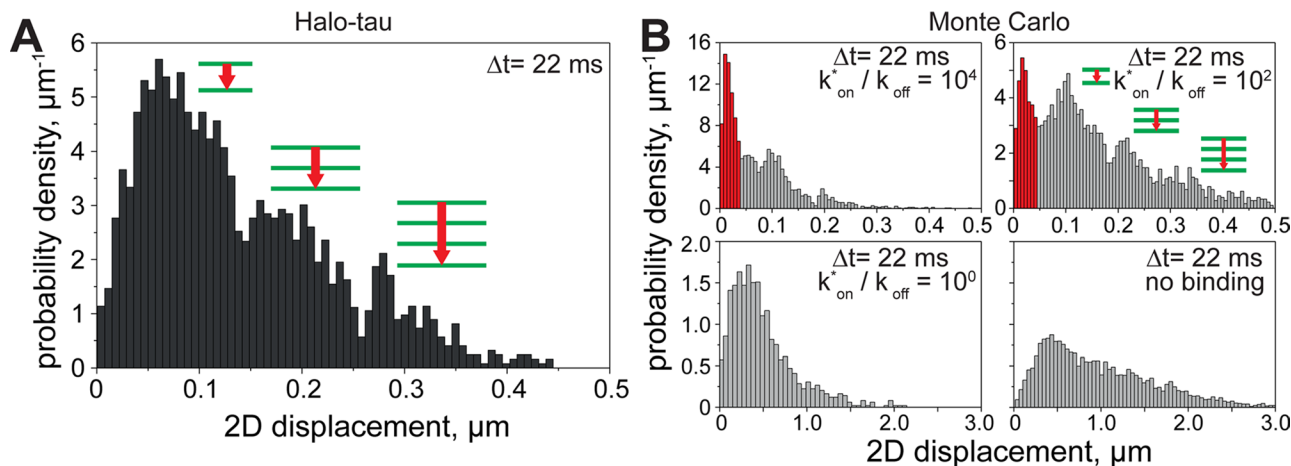


FIGURE 3: Step-size distribution analysis and Monte Carlo simulation indicate jumps of tau between microtubules. (A) SSD analysis of >1000 pseudotrajectories indicating subpopulations of jumps between MTs. The peaks in the histogram correspond to 1 → 2, 1 → 3, and 1 → 4 hops between MTs. (B) SSD analysis of simulated pseudotrajectories at different pseudoequilibrium constants (k_{on}^*/k_{off}). Note that the histogram at $k_{on}^*/k_{off} = 10^2$ closely resembles the data shown in A. The Monte Carlo simulation revealed an additional peak (indicated in red), which was not resolved by imaging.

multiple binding partners within a few tens of milliseconds. Note that peaks at intermediate locations, which might be expected due to different z-positions of neighboring MTs, are merged due to the 2D projection and contribute to the widening of the peaks.

To validate this result, we simulated by Monte Carlo algorithm the hopping of tau in a cellular process filled with microtubules. Two input parameters were fixed, namely, the diffusion constant of free tau ($14.4 \mu\text{m}^2/\text{s}$; see *Materials and Methods*) and the average spacing of MTs of 70 nm. The rate constants for association and dissociation of tau were varied (Figure 3B). The simulated SSD resembles the data shown in Figure 3A for $k_{on}^*/k_{off} = 10^2$. This value implies 99% of tau being bound, which is compatible with data on tau–MT binding from cell-free experiments at cellular tubulin concentration (Brandt and Lee, 1993b). In vitro, tau binds to microtubules with relatively weak affinity ($K_d = 1.1 \times 10^{-7} \text{ M}$; Butner and Kirschner, 1991) and the saturating molar ratio measured for tau protein binding to polymer-

ized tubulin has been determined as 1:5 (Cleveland *et al.*, 1977; Hirokawa *et al.*, 1988). On the basis of these numbers, one calculates k_{on}^*/k_{off} as ~ 50 , which is also close to the ratio where the simulation revealed peaks. Note that the simulation revealed an additional peak at $\sim 20 \text{ nm}$. This peak represents hops between MTs whose projections on the 2D plane closely neighbor but can be more distant in three dimensions. This peak remains unresolved in the experiment because it was close to the localization precision of $\sim 20 \text{ nm}$.

Single-molecule experiments allow estimating the dwell time of tau on a single microtubule. The respective frequency histograms of residence times of tau on MTs could be best fitted to a single exponential, indicating that tau has only one major interaction partner in neuritic shafts, namely, MTs. Time constants of the exponential fits were referred to as dwell times (Figure 4). We found that tau dwells on a single MT for $\sim 40 \text{ ms}$, which is shorter by two orders of magnitude than previously reported (Konzack *et al.*, 2007).

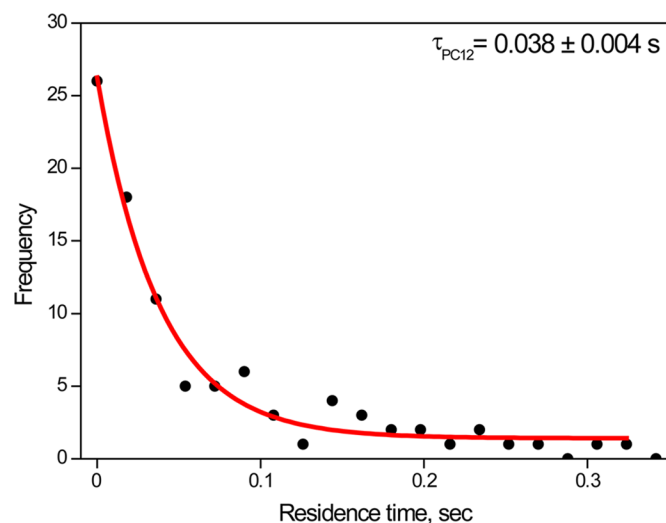


FIGURE 4: Representative histogram of residence times of tau on microtubules in PC12 cells. The monoexponential fit is shown by a red line, and the time constant (dwell time) is indicated on top.

Tau promotes microtubule assembly despite its rapid kiss-and-hop dynamics

The data show that tau only briefly resides on one particular MT until it hops to a neighboring one. We asked whether this short-lived interaction is compatible with an effect of tau on microtubule polymerization in living cells. To address this question, we coexpressed mCherry-tagged tau or, as a control, 3xmCherry together with PAGFP-tagged α -tubulin in neuronally differentiated PC12 cells. Tau-induced changes in MT dynamics were then monitored by FDAP measurements from cells in which the fluorescence of PAGFP had been focally activated in the middle of a process (Gauthier-Kemper *et al.*, 2012; Figure 5, A and B). The normalized intensity of the control (3xPAGFP) showed a considerably faster decay than that of α -tubulin (Figure 5C), indicating reaction-dependent diffusion of tubulin versus free diffusion of 3xPAGFP. The presence of mCherry-tau significantly slowed the decay of α -tubulin, whereas 3xmCherry did not have any effect (Figure 5C, left vs. right). To determine the fractions of free and bound tubulin, we fitted the FDAP curves to a reaction-diffusion model (see *Materials and Methods*). In the absence of exogenous tau, about two-thirds of PAGFP-tubulin was polymerized in the cell processes. The exogenous mCherry-tau increased

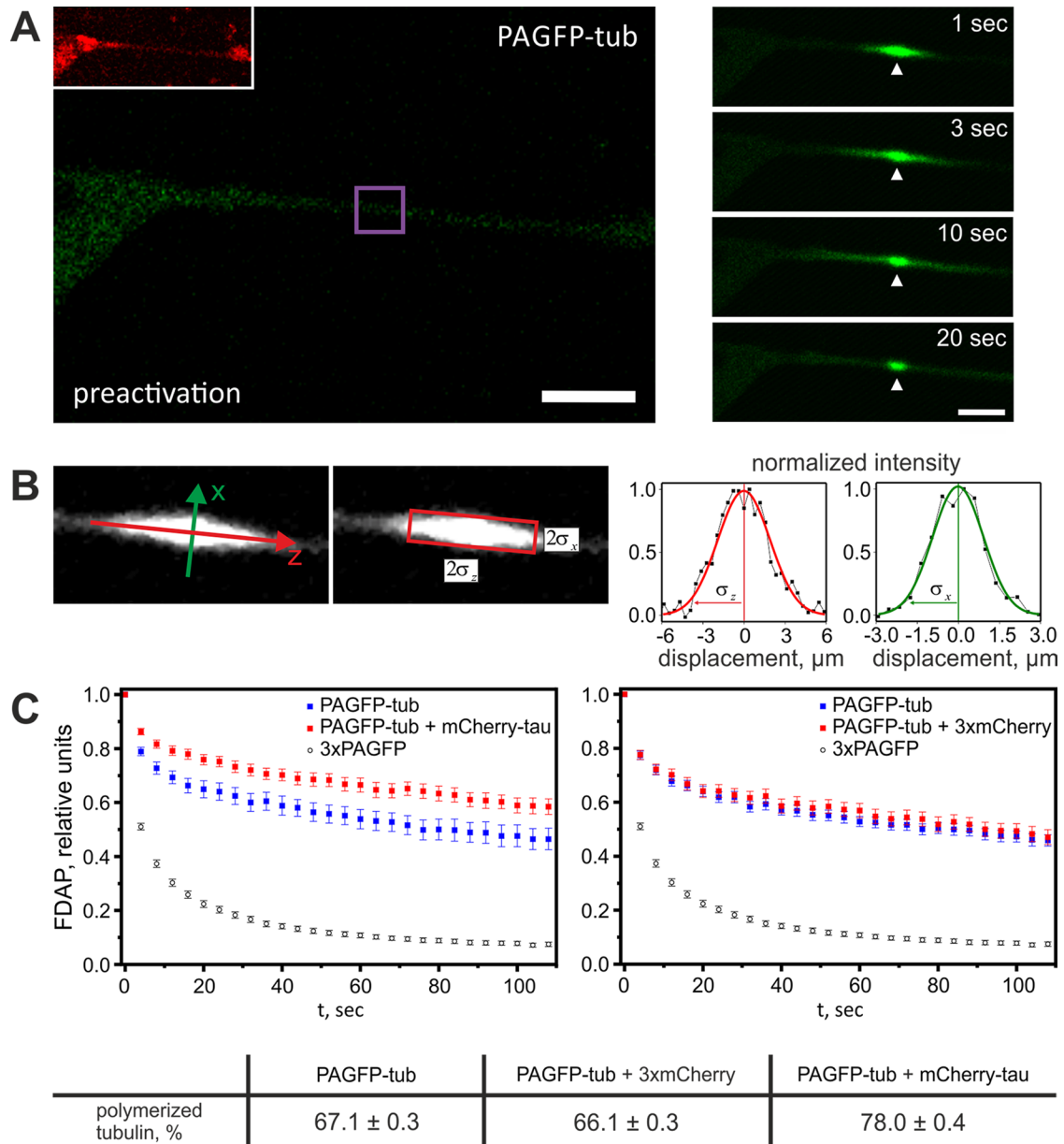


FIGURE 5: Tau promotes microtubule assembly in neurites of living cells. (A) Live-cell imaging of a PC12 cell coexpressing mCherry-tagged tau (left, inset) and PAGFP-tagged α -tubulin (PAGFP-tub) before and after fluorescence photoactivation. The position of activation is indicated by a violet box. Fluorescence decay of PAGFP-tub in the activated region is indicated by the arrows. Scale bar, 10 μ m. (B) Determination of the axes of symmetry (left) and the plot of normalized intensity distributions (right) as they were used to define the ROI. (C) FDAP curves of PAGFP-tub in the ROI. The presence of mCherry-tau decreases fluorescence decay of PAGFP-tub (left), whereas a control protein (3xmCherry) has no effect (right). For comparison, FDAP of a soluble protein (3xPAGFP) is shown. Values are expressed as mean \pm SEM ($n = 29$ – 36). Fractions of polymerized PAGFP-tub were estimated based on fitting of the respective FDAP curves to a reaction-diffusion model (bottom).

polymerization by $\sim 10\%$ (Figure 5C, bottom). This was consistent with previous results from *in vitro* experiments, in which tau was shown to induce microtubule polymerization in a concentration-dependent manner (Brandt and Lee, 1993a). Taken together, the data indicate that tau is capable of promoting MT assembly in neurites despite its rapid kiss-and-hop dynamics. However, it should be taken into account that the experiment uses an overexpression system in which tubulin and tau are expressed on top of the respective endogenous proteins. It remains to be shown whether it is also the physiological function of tau to promote microtubule assembly in neurites.

Tau exhibits kiss-and-hop behavior also in axons of primary neurons

PC12 cells are a well-characterized neuronal model with a rather homogeneous cell population and well-defined microtubule distribution in processes. They do not, however, develop axonal-somatodendritic polarity. To examine the behavior of tau in axons, we prepared primary mouse cortical cultures and introduced Halo-tagged tau by lentiviral gene transfer (Bakota *et al.*, 2012; Figure 6A, left). To avoid potential interference of endogenous mouse tau, we prepared cultures from *TAU^{-/-}* animals. A Western blot

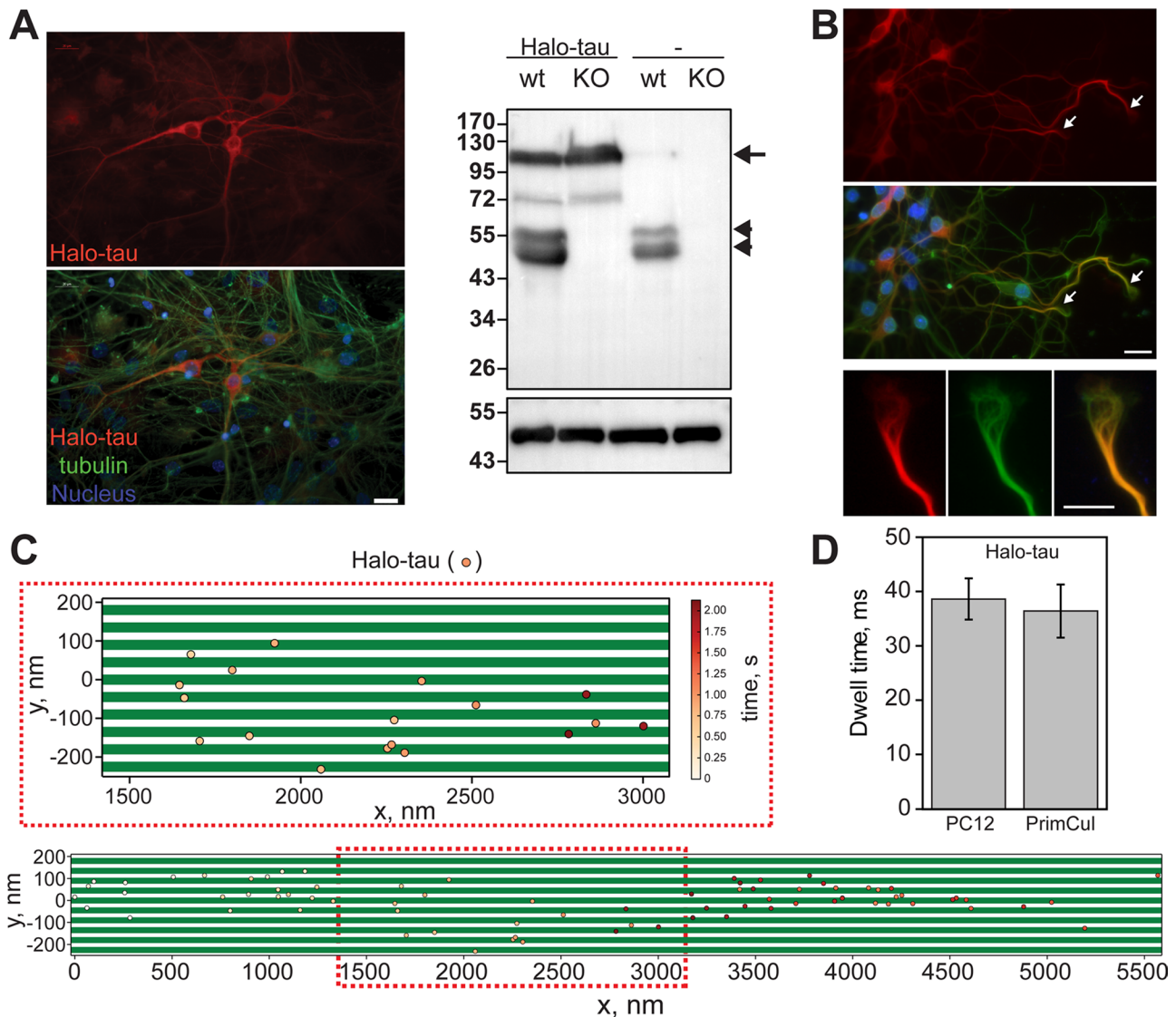


FIGURE 6: Tau exhibits kiss-and-hop behavior also in axons of primary neurons. (A) Triple fluorescence micrographs showing expression of Halo-tau (red) in lentivirally infected wild-type mouse cortical neurons. Staining against tubulin (DM1A, green) and nuclei (4',6-diamidino-2-phenylindole [DAPI], blue) is shown. Right, Western blot indicating expression of exogenous Halo-tau (arrow) in cultures from wild-type (wt) or $TAU^{-/-}$ mice (KO). The presence of endogenous tau in wt mice is indicated by arrowheads. Bottom, staining for actin as a loading control. Scale bar, 20 μ m. (B) Triple fluorescence micrographs after a fixation-extraction protocol, which reveals cytoskeletal association. Cortical neurons from $TAU^{-/-}$ mice were lentivirally infected to express Halo-tau (red). Top, overview; bottom, individual growth cone region. Note the enrichment of Halo-tau at the transition between the axon shaft and the growth cone as indicated by arrows. Staining against tubulin (DM1A, green) and nuclei (DAPI, blue) is shown. Scale bar, 20 μ m (top), 10 μ m (bottom). (C) Localization of a single Halo-tau molecule in an axon of a $TAU^{-/-}$ neuron over time. For comparison, thickness and density of axonal MTs are schematically indicated by the green bars. Top, enlargement of the indicated segment. Note that the MT–MT distance in axons of cortical neurons is much smaller than in neurites of PC12 cells. (D) Dwell times of Halo-tau in neurites of PC12 cells (39 ± 4 ms; $n = 7$) and axons of primary cultures (36 ± 5 ms; $n = 4$). Data represent mean \pm SEM.

confirmed 1) the absence of endogenous mouse tau in the $TAU^{-/-}$ cultures (arrowheads, Figure 6A, right) and 2) the expression of Halo-tau at a level comparable to that of the endogenous one (arrow, Figure 6A, right).

Halo-tau was ubiquitously present in the neurons, similar to what has been observed after expression of exogenous tau in cultured neurons or transgenic animals (Konzack *et al.*, 2007; Hundelt *et al.*, 2011). This might be due to the fact that the expression constructs lack the 3' untranslated region of the tau mRNA, which targets the mRNA to the proximal axon (Litman *et al.*, 1993; Aronov *et al.*, 2001). To prove that Halo-tau binds to axonal microtubules, we used a

previously described extraction-fixation protocol to visualize tau's microtubule interaction. We observed that Halo-tau clearly associated with axonal MTs (Figure 6B). Furthermore, binding was highest at the transition between the axon shaft and the growth cones (Figure 6B, arrows), similar to what was previously observed for endogenous tau in cultured neurons (Kempf *et al.*, 1996). Thus the experimental approach appears to be appropriate to analyze the mode of the interaction of tau with axonal microtubules. Note that primary neurons have a much higher density of MTs in their axons than is present in the processes of PC12 cells. The typical axonal MT–MT distance was reported to be ~ 20 nm (Hirokawa and

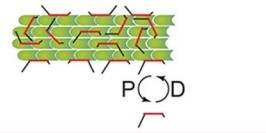
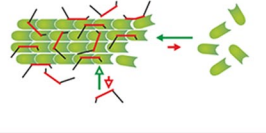
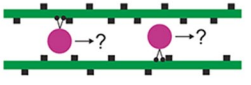

	Standard model	New model
Dwell time	~4 s	~40 ms
MT regulation	phosphorylation/dephosphorylation cycles	kiss-and-hop
Kinetics		
Transport		

FIGURE 7: Schematic representation illustrating features and consequences of the kiss-and-hop behavior of tau as identified in this study. P, phosphorylation; D, dephosphorylation.

Takemura, 2005). However, despite this difference, a representative 2D projection of binding positions of a single tau molecule revealed very similar kiss-and-hop behavior, indicating that it is independent of MT density and the presence of endogenous tau (Figure 6C and Supplemental Movie S5). Moreover, we found a dwell time of ~40 ms on the MT surface (Figure 6D; see *Materials and Methods*). Therefore there was no significant difference between the dwell times of tau molecules in processes of PC12 cells and axons of primary cultures.

DISCUSSION

The foregoing data represent the first recording on a single-molecule level of the interaction of a structural MAP with the MT network in living neurons. The major findings are the following: 1) the dwell time of bound tau on each MT filament (~40 ms) is shorter by two orders of magnitude than previously believed (Konzack *et al.*, 2007), 2) tau hops between MTs in an undirected manner, and 3) despite its high mobility, tau is capable of shifting the equilibrium between free tubulin and the MT network toward polymerization.

Our findings have several consequences for the physiological role of tau (schematized in Figure 7). In vivo the velocity of axonal transport is virtually unaffected by tau (Yuan *et al.*, 2008), which is fully compatible with its kiss-and-hop kinetics. Indeed, knowing the concentration of tau molecules in neurons and the ratio of bound molecules, one calculates the mean lateral distance between the two closest tau molecules bound to the same MT simultaneously to be ~45 nm (see *Materials and Methods*). Kinesins move on the MT surface with an average velocity of ~1 $\mu\text{m/s}$ (Kaether *et al.*, 2000). During the mean dwell time of tau (~40 ms), they progress by ~40 nm. Therefore kinesins can readily proceed on the MT without being impeded by tau standing in their way. If the dwell time was much longer, tau, which shares binding sites with kinesins on MTs (Seeger and Rice, 2010), would impair the axonal transport. It is noteworthy that the rapid dynamic behavior of tau is also compatible with its non-MT-related functions and its multiple interactions in the cell (Morris *et al.*, 2011).

The view that tau binding to MTs is regulated by phosphorylation and dephosphorylation cycles (Ballatore *et al.*, 2007) obviously conflicts with tau's rapid dynamic behavior. The catalytic rate of a typical protein kinase is ~10 reactions/s (Newton, 1995). Given the average number of MT interactions that a single tau molecule experiences per second (~2000 reactions/s), phosphorylation cannot directly modulate the rapid tau-MT binding kinetics within one phosphorylation cycle.

We provided evidence that tau is capable of promoting MT assembly in neurites despite its rapid kiss-and-hop dynamics.

According to a study by Gardner *et al.* (2011), the MT self-assembly kinetics is strongly dependent on the concentration of free tubulin subunits and is an order of magnitude more rapid than previously believed (the lifetime of a tubulin subunit in a GTP cap is ~1 ms at the physiological concentration of tubulin subunits). It appears unlikely that such a dynamic system as the MT network is regulated by a MAP whose dwell time on MTs is in the range of several seconds. This rapid MT kinetics also implies that even a weak suppression of the tubulin off-rate strongly affects catastrophe and rescue events in the axon. Our data suggest a new mechanism of axonal MT regulation by tau, namely, the short interaction of tau with

MTs (~40 ms) suppresses the natural rapid dissociation of tubulin dimers at the MT tip, leading to an increase of the MT GTP cap size. It is noteworthy that such a function of tau is fully compatible with its distribution in the axon, since we observed that the association of tau with the cytoskeleton is highest at the transition between the axon shaft and the growth cone (Figure 6B), where microtubules are known to be most dynamic.

Thus the revealed dwell time of tau (~40 ms) appears optimal for the following two reasons. On the one hand, it is short enough not to inhibit axonal transport, and on the other hand, it is long enough to regulate MT dynamics. Pathological shifts in tau's MT association or dwell times (e.g., induced by long-term abnormal phosphorylation of tau) may provoke changes in the dynamic equilibrium of tau with MTs and hence result in a disturbed tubulin-MT equilibrium.

MATERIALS AND METHODS

Materials and antibodies

Chemicals were obtained from Sigma-Aldrich (Deisenhofen, Germany), cell culture media and supplements were obtained from Sigma-Aldrich and Invitrogen, and culture flasks, plates, and dishes were obtained from Thermo Fisher Scientific (Schwerte, Germany), unless stated otherwise. The following antibodies were used: anti-tubulin (mouse, DM1A), Tau5 (mouse; BD Biosciences, Heidelberg, Germany) and anti-actin (mouse; Calbiochem/Merck, Darmstadt, Germany). As secondary antibodies, peroxidase- and Alexa Fluor 488-conjugated anti-mouse antibodies (Jackson ImmunoResearch Laboratories, West Grove, PA) were used.

Construction of expression vectors, transfections, and lentiviral infections

For bright and highly photostable signals from single tau molecules during live-cell imaging, we used the enzymatic HaloTag system and the HaloTag TMR ligand (Los *et al.*, 2008). The eukaryotic expression plasmid for adult (441 amino acids) human tau with aminoterminally fused HaloTag tag were constructed from pRc/cytomegalovirus (CMV)-htau441wt expression vectors (Gauthier-Kemper *et al.*, 2011) by addition of restriction sites *NotI* and *XhoI* flanking to tau. The resulting PCR product was sequentially cut with the respective enzymes (Fermentas, St. Leon-Rot, Germany) and cloned into pSems-Halo-1-26m (Wilmes *et al.*, 2012). For generating pSems-mEGFP- α -tubulin the respective α -tubulin sequence was amplified by PCR from pIREShyg-PAGFP- α -tubulin (Tulu *et al.*, 2003; plasmid 12296; Addgene) and inserted into pSems-mEGFP restricted by *BamHI* and *NotI* (Wilmes *et al.*, 2012). Synaptophysin-mCherry was synthesized with the restriction sites *BamHI* and *XbaI*

from Life Technologies (Darmstadt, Germany) and cloned into pRC/CMV (Gauthier-Kemper *et al.*, 2011). The pCMV-3xPAGFP plasmid was described previously (Weissmann *et al.*, 2009).

To obtain the L22-3xmCherry construct, named pJH1392, in vivo recombination was used employing triple mammalian/yeast/bacterial shuttle vectors as described previously (Bakota *et al.*, 2012). Specifically, the coding sequence for 3xmCherry was PCR amplified from pJH1255, a derivative of pCM79, kindly provided by M. Knop (University of Heidelberg, Germany; Maeder *et al.*, 2007), using the oligonucleotide pair 11.357/11.358 (AATCTTTCACAAATTTG-TAATCCAGAGGTTGATTATCGATAAGAAGTGGCGCGCTCACTC-GAG, TAGTTCTGGGGCAGCGGGGATCCCCGGTACCGGTCCACCGAAGCTTCGTACGCTGCAGG). The PCR product was cotransformed into the diploid yeast strain DHD5 with pJH1308 linearized with *Bam*HI and selected for growth on medium lacking uracil (Bakota *et al.*, 2012). Isolation of plasmid DNA, amplification in *Escherichia coli*, and sequencing confirmed that the recombination occurred as expected. For construction of the L22-mCherry-htau441wt viral vector, named pJH1311, a similar strategy was followed based on in vivo recombination with pJH1308 linearized with *Bam*HI. As a template to obtain the mCherry-htau441wt coding sequence, we used pJH1309 with the oligonucleotide pair 11.045/11.046 (GGGCAGGCGAGTGGCCCTAGTTCTGGGGCAGCGGGGATATGGTGAGCAAGGGCGAGGAGG, AGGTTGATTATCGATAAGCTTGATATCGAATTCTAGAaccggtgcgcgatcCGACCTATCACAACCCTGC, with the lowercase letters indicating sequences inserted for introduction of restriction sites, which appear neither in the template nor in the recipient vector). pJH1309 was also obtained by in vivo recombination with linearized pJH900 (containing a Flag-htau441wt sequence cloned under the control of the yeast *GAL1/10* promoter as a *Bam*HI/*Sph*I fragment into pJH447; Lorberg *et al.*, 2001). The mCherry sequence was introduced as a PCR product using pAJ001 (Jendretzki *et al.*, 2009) as a template with the oligonucleotides 11.043/11.044 (ATCCAAAAAAGTAA-GAATTTTTGAAAATCAATATAAATGGTGAGCAAGGGCGAGGAGG; CGAACTCCTGGCGGGGCTCAGCCATCGATTTATCGTCATCCTTGACAGCTCGTCCATGCCGCC) and substituted the Flag tag in pJH900. pJH1311 was then linearized with *Sbf*I, and the mCherry sequence was substituted for a Halo-tag by in vivo recombination in yeast with a PCR product obtained from pSems-Halo-tau using the oligonucleotides 11.037/11.519 (cgcgCTCGAGTTTCAG-GCCAGCGTCCGTGTAC, binding with the uppercase letter sequences within the tau sequence, and AGCACGGGCGAGCGAGTGGCCCCTAGTTCTGGGGCAGCGGGGAATGGGATCGAAATCGGTACTGG, which provides the homology to the *Cam*KII promoter in the vector sequence). The resulting mCherry-htau441 construct was named pJH1440 and used to generate viral vectors.

Transfections of PC12 cells were performed with Lipofectamine 2000 (Invitrogen) essentially as described previously (Fath *et al.*, 2002). For production of lentivirus, human embryonic kidney cells 293FT (Invitrogen) were transfected with the expression vector, and two helper plasmids and viral particles from the supernatant were concentrated by ultracentrifugation as described previously (Bakota *et al.*, 2012).

Cell culture and live-cell labeling

PC12 cells were cultured in serum-DME as described previously (Fath *et al.*, 2002). Undifferentiated cells were plated on 35-mm poly-L-lysine- and collagen-coated glass-bottom culture dishes (MatTek, Ashland, MA) at 10^3 cells/cm² and cultured in DME with 1% (vol/vol) serum. For TIRF imaging, cells were plated on glass coverslips (24 mm, No. 1; VWR, Radnor, PA) that were coated with a

poly-L-lysine-graft-(polyethylene glycol) copolymer functionalized with RGD as described previously (VandeVondele *et al.*, 2003). Cells were flattened by addition of 100 ng/ml 7S mouse nerve growth factor (NGF; Alomone Laboratories, Munich, Germany) for 1–2 d. For neuronal differentiation, NGF treatment was extended to 4–6 d, and the medium was changed every 2–3 d. Before imaging, the medium was exchanged against the same medium containing DME without phenol red. Primary cortical cultures were prepared from cerebral cortices of mouse embryos (days 14–16 of gestation) and cultured as described previously (Bakota *et al.*, 2012). The cultures were obtained from C57BL/6 and *TAU*^{-/-} mice (Dawson *et al.*, 2001). Cells were plated at 2.5×10^4 cells/cm² on polylysine- and laminin-coated coverslips.

Labeling of PC12 cells and primary cultures was performed by incubation with serum-DME containing 1–5 nM TMR-HTL for 15 min at 37°C. This corresponded to a labeling efficiency of <0.02% of the exogenous Halo-tau. Subsequently, cells were washed with serum-DME without phenol red and then left to recover for 1/2 h in the incubator, followed by an additional medium exchange. All animals were maintained and killed according to National Institutes of Health guidelines and German animal care regulations.

Immunocytochemistry

Immunocytochemistry after fixation with 4% paraformaldehyde and a combined NP-40 detergent extraction-fixation procedure to reveal cytoskeletal association were performed as described previously (Gauthier-Kemper *et al.*, 2011). Fluorescence microscopy used a dry 40x (numerical aperture [NA] 0.75) objective lens on a fluorescence microscope (Eclipse TE2000-U; Nikon, Tokyo, Japan) equipped with a digital camera (COOL-1300; Vosskühler, Osnabrück, Germany). Image analysis used the program Lucia G (Nikon).

Photoactivation and live imaging

Live imaging was performed on a laser scanning microscope (Eclipse TE2000-U inverted; Nikon) equipped with argon (488 nm), helium/neon (543 nm), and blue diode (405 nm) lasers. PAGFP-tubulin expressing cells were visualized with a Fluor 60x (NA 1.4) ultraviolet-corrected (VC) objective lens. The microscope was enclosed in an incubation chamber maintained at 37°C and 5% CO₂ (Solent Scientific, Fareham, UK). Automated image acquisition after photoactivation was essentially performed as described previously (Weissmann *et al.*, 2009). Photoactivation was performed with the blue diode, producing an activation spot 5 μm in diameter. Frames were obtained at a frequency of 1 frame/s, and 112 frames were collected per experiment. Standard series were collected at a resolution of 256 × 256 pixels.

Single-molecule microscopy, localization, and tracking

For recording single molecules, TIRF microscopy was performed using an Olympus excellence cell[^]TIRFM microscope equipped with 405-nm (200 mW), 488-nm (200 mW), 561-nm (200 mW), and 647-nm (140 mW) lasers (Olympus, Tokyo, Japan), as well as a backilluminated electron multiplied charge-coupled device camera (C9100-13; Hamamatsu, Hamamatsu City, Japan). Fast single-molecule tracking used a digital complementary metal-oxide-semiconductor camera (ORCA-Flash4.0 V2 C11440-22CU; Hamamatsu). A 150x magnification objective with NA 1.45 (UAPON 150x/1.45, Olympus) was used for TIR illumination. The excitation beam was reflected into the objective by a quad-line dichroic beam splitter for reflection at 405, 488, 568, and 647 nm (DiO1 R405/488/561/647; Semrock, Rochester, NY). The emitted light from the sample was filtered using a quad-band bandpass filter (FF01 446/523/600/677; Semrock). The

microscope was enclosed in an incubation chamber maintained at 37°C and 5% CO₂ (Olympus).

Localization of single molecules and single-molecule tracking were carried out as previously described (Hess *et al.*, 2006; Sergé *et al.*, 2008; Wilmes *et al.*, 2012). The theoretical localization precision of Halo-tau and syp-mCherry was 16.7 ± 0.2 and 14.2 ± 0.2 nm, respectively. For further analysis, a mask was placed over the processes, and localizations/trajectories outside of this mask were removed. In addition, all trajectories were aligned with the horizontal axis.

SSD analysis

SSDs were calculated as described before (Weimann *et al.*, 2013). To exclude potential false connections produced by the tracking algorithm, we restricted the duration of the trajectories to the first three steps. The obtained shortened trajectories were used to plot the SSDs for the first time step, $t = \Delta t$.

Dwell-time determination

The dwell time of tau using single-molecule localizations was determined by counting how many consecutive frames a single localized signal stayed within a radius of 50 nm. The respective frequency histograms were fitted to a single exponential to obtain the dwell time.

FDAP data analysis

To plot normalized decay curves, we first extracted the first frame from the image sequence and chose the region of interest (ROI) containing a part of the cellular process with the desired intensity distribution $I(x, y)$. The image was thresholded to suppress the background noise, and the axes of symmetry of $I(x, y)$ were found. The longitudinal (along the process) and transversal (across the process) axes were then used to plot the intensity profile distributions. The distributions were fitted to slightly modified Gaussian profiles:

$$\begin{aligned} f(x) &= f_{x0} + A_x \exp\left(\frac{-2x^2}{\sigma_x^2}\right) \\ g(y) &= f_{y0} + A_y \exp\left(\frac{-2y^2}{\sigma_y^2}\right) \end{aligned} \quad (1)$$

where f_{x0} and f_{y0} are offset parameters and $A_x > 0$ and $A_y > 0$ are the maximal amplitudes of the intensity profiles. The parameters $\sigma_x > 0$ and $\sigma_y > 0$ represent the spatial half-widths of the longitudinal and transversal distributions, respectively. Then we used σ_x and σ_y to define the recording area—a rectangle with the sides $2\sigma_x$ in length and $2\sigma_y$ in width. The average intensity was then acquired from the recording area. More than 20 independent FDAPs for PAGFP-tub coexpressed with either 3xmCherry or mCherry-tau were performed to form the final single FDAP curves. In all cases, the preactivation frame was subtracted from the rest of the frames in order to exclude the preactivation fluorescence from the desired signal. The obtained raw curves were then averaged and normalized on the maximal intensity.

Monte Carlo simulations of tau dynamics

We simulated tau's reaction-diffusion dynamics in a process of a PC12 cell. The simulation space was defined as a tube of length $L = 100 \mu\text{m}$ and radius $R = 500 \text{ nm}$. The tube was filled with 60 parallel MTs of $R_{\text{MT}} = 12.5 \text{ nm}$, with an intermicrotubule distance of 70 nm. The geometry chosen was in good correspondence with the actual one revealed by Jacobs and Stevens (1986) for cellular processes of PC12 cells after 4 d of NGF treatment. At the initial moment, 1000 particles were randomly positioned within the simulation space. Each particle had a probability $k_{\text{on}}^*/(k_{\text{on}}^* + k_{\text{off}})$ of being bound to a MT and a probability $k_{\text{off}}/(k_{\text{on}}^* + k_{\text{off}})$ of being placed anywhere in the cytosol.

Once the geometry and the populations had been set, the time loop was started. The time step was equal to $\Delta t = 1 \mu\text{s}$. At each time step, each bound particle had a probability p_{off} of unbinding. In case it was decided for unbinding, the detachment of the particle occurred in the direction locally perpendicular to the MT surface to which this particle was attached. On the contrary, each free particle was first checked for the act of hitting a MT surface. When hit, the particle had a probability p_{on} of being attached. In case of not attaching, the particle again came off in the direction locally perpendicular to the surface. If the free particle did not hit a MT surface or failed attaching to it and came off, a random displacement ($\Delta x, \Delta y, \Delta z$) for this particle was generated. The displacements $\Delta x, \Delta y$, and Δz were calculated as normally distributed random numbers with the SD equal to $\sqrt{2D\Delta t}$, where D is the diffusion constant. Reflection boundary conditions at the outer boundary of the simulation space were imposed. The procedure was iterated for 10^6 – 10^7 time steps.

Diffusion constant estimation for PAGFP-htau and PAGFP-tub

The Stokes–Einstein equation, $D = k_B T / 6\pi\eta R_H$, for diffusion of spherical particles in liquid with low Reynolds numbers was used to estimate diffusion constants. In this formula, k_B is the Boltzmann constant, T is absolute temperature of the surrounding medium, η is the viscosity of the medium, and R_H is the hydrodynamic radius of the molecule of interest. We assumed the medium to have a viscosity of 3.4 cP at $T = 310 \text{ K}$, as previously measured for the cytosol of neuronal processes (Popov and Poo, 1992). The hydrodynamic radius, in turn, depends on the structural properties of the molecule of interest. First, we estimated the diffusion constant for GFP and its derivatives (enhanced GFP, PAGFP). According to Hink (2000), the hydrodynamic radius of GFP is $\sim 2.3 \text{ nm}$. This is in good correspondence with an empirical formula for globular proteins, $R_H = 0.595M^{0.427}$ (mass in kilodaltons), which yields 2.4 nm for 27-kDa mass of GFP. This radius corresponds to $D = 28 \mu\text{m}^2/\text{s}$. Several research groups have reported various experimental estimates for the diffusion constant of GFP in different cellular compartments (Swaminathan *et al.*, 1996; Hink, 2000; Sprague *et al.*, 2004; Michelman-Ribeiro *et al.*, 2009). These values varied from 15 to $27 \mu\text{m}^2/\text{s}$. Our FDAP experiments yielded a consensus value of $\sim 20 \mu\text{m}^2/\text{s}$ for PAGFP based on the measurements for 3xPAGFP ($D = 13.9 \pm 1.0 \mu\text{m}^2/\text{s}$) in processes of neuronal PC12 cells and subsequent recalculation for a smaller mass, since $D \sim M^{-1/3}$. We then estimated the diffusion coefficient for htau alone, which has a molecular weight of 45.85 kDa. Previous small-angle x-ray scattering experiments revealed a radius of gyration of 6.5 nm for 441-residue htau (Mylonas *et al.*, 2008). The ratio of the radius of gyration to the hydrodynamic radius lies in the range 1.2–1.5 for intrinsically disordered proteins (Mukrasch *et al.*, 2009), thus yielding $R_H = 5.4 \text{ nm}$ for htau. This value is in accordance with the value of 5.76 nm given by an empirical formula for random coils (Mylonas *et al.*, 2008), $R_G = 0.1927n^{0.588}$, where n is the number of residues, although htau is not completely unstructured. The experimental estimate for the hydrodynamic radius of htau hence gives a diffusion constant of $\sim 12 \mu\text{m}^2/\text{s}$. Finally, we estimated the diffusion constant for PAGFP-htau. To our knowledge, the hydrodynamic radius for this fusion has not been measured experimentally. However, we estimated maximal and minimal values R_H can take. The maximal value follows from the assumption that the fusion PAGFP-htau is completely unstructured. Using the empirical formula for random coils yields $R_{H,\text{max}} = 7.4 \text{ nm}$. The minimal value $R_{H,\text{min}} = 3.7 \text{ nm}$ follows from the empirical formula for globular proteins. Thus the actual diffusion constant for PAGFP-htau should be between 9 and

18 $\mu\text{m}^2/\text{s}$. On the basis of $D = 13.9 \pm 1.0 \mu\text{m}^2/\text{s}$ for 3xPAGFP, we recalculated the diffusion constant for PAGFP-htau ($D_{\text{PAGFP-htau}} = D_{3\text{xPAGFP}} \sqrt[3]{M_{3\text{xPAGFP}}/M_{\text{PAGFP-htau}}}$), which was equal to $\sim 14.4 \mu\text{m}^2/\text{s}$.

We used the same strategy to estimate the diffusion coefficient for PAGFP-tub, which after forming a dimer with endogenous β -tubulin has a mass of 137 kDa. However, unlike htau, tubulin is a globular protein, which encourages use of the empirical formula for globular proteins to estimate D for PAGFP-tub. Doing so yields $\sim 14 \mu\text{m}^2/\text{s}$. Previous measurements using injection of rhodamine-labeled tubulin into squid giant axons gave $D = 8.6 \mu\text{m}^2/\text{s}$ (Galbraith *et al.*, 1999). Using the diffusion constant of 3xPAGFP ($D = 13.9 \pm 1.0 \mu\text{m}^2/\text{s}$), we get $11.8 \mu\text{m}^2/\text{s}$ for PAGFP-tub ($D_{\text{PAGFP-tub}} = D_{3\text{xPAGFP}} \sqrt[3]{M_{3\text{xPAGFP}}/M_{\text{PAGFP-tub}}}$).

Reaction-diffusion model for FDAP

We consider a photoactivatable molecule that diffuses in an infinite cylinder with a diffusion constant D and obeys first-order kinetics,



where C represents the free molecule species at concentration c , B represents binding sites at concentration b , and S represents the bound molecular species at concentration s . We make the following assumptions:

- 1) Before the photoactivation, the molecular ensemble has reached equilibrium with its binding sites, and the equilibrium concentrations c_{eq} , b_{eq} , and s_{eq} have been settled.
- 2) The photoactivation does not disturb the concentration of binding sites ($b = b_{\text{eq}}$).
- 3) Diffusion is one dimensional and proceeds along the longitudinal axis Oz . The lateral diffusion is negligible.
- 4) The molecule of interest diffuses only when free in cytosol.
- 5) The PAGFP tag does not affect binding.

The reaction-diffusion equations then read as follows:

$$\begin{aligned} \frac{\partial c}{\partial t} &= D \frac{\partial^2 c}{\partial z^2} - k_{\text{on}}^* c + k_{\text{off}} s \\ \frac{\partial s}{\partial t} &= k_{\text{on}}^* c - k_{\text{off}} s \end{aligned} \quad (3)$$

where $k_{\text{on}}^* = k_{\text{on}} b_{\text{eq}}$ is the pseudo-first-order association rate. The relative equilibrium concentrations are given by

$$\bar{c}_{\text{eq}} = \frac{c_{\text{eq}}}{c_{\text{tot}}} = \frac{1}{1 + k_{\text{on}}^*/k_{\text{off}}}, \quad \bar{s}_{\text{eq}} = \frac{s_{\text{eq}}}{c_{\text{tot}}} = \frac{k_{\text{on}}^*/k_{\text{off}}}{1 + k_{\text{on}}^*/k_{\text{off}}}, \quad c_{\text{tot}} = c_{\text{eq}} + s_{\text{eq}} \quad (4)$$

where c_{tot} is the total concentration of the molecules of interest. Here we derive the solutions to the system of Eqs. 3 for two simplified cases. The first case relates to pure diffusion, that is, to a scenario when the majority of molecules are free ($c_{\text{eq}} > s_{\text{eq}}$). In this case, the system of Eqs. 3 reduces to a simple diffusion equation,

$$\frac{\partial c}{\partial t} = D \frac{\partial^2 c}{\partial z^2} \quad (5)$$

This scenario is supposed to describe a freely diffusing protein like 3xPAGFP. The second case concerns a scenario in which diffusion is very fast compared with the time scale of reaction ($\tau_D \ll 1/k_{\text{on}}^*$, where τ_D is the characteristic time scale of diffusion over the activation region). Thus diffusion and binding are largely separable processes, and the free and bound molecules behave as uncoupled species. The system of Eqs. 3 then turns into

$$\begin{aligned} \frac{\partial c}{\partial t} &= D \frac{\partial^2 c}{\partial z^2} \\ \frac{\partial s}{\partial t} &= -k_{\text{off}} s \end{aligned} \quad (6)$$

This scenario is expected to describe the behavior of PAGFP-tub. In the FDAP experiment, such behavior was typical (Figure 5A). We then calculate the theoretical expression for the normalized FDAPs defined as $FDAP(t) = (1/2\sigma) \int_{-\sigma}^{\sigma} [c(z, t) + s(z, t)] dz$ (where 2σ is the width of the photoactivation region) for the two simplified scenarios:

$$\begin{aligned} FDAP_{\text{pure}}(t) &= \text{erf} \sqrt{\frac{\tau_D}{t}} + \sqrt{\frac{t}{\pi \tau_D}} \left(\exp\left(-\frac{\tau_D}{t}\right) - 1 \right) \\ FDAP_{\text{reaction}}(t) &= \bar{c}_{\text{eq}} \left(\text{erf} \sqrt{\frac{\tau_D}{t}} + \sqrt{\frac{t}{\pi \tau_D}} \left(\exp\left(-\frac{\tau_D}{t}\right) - 1 \right) \right) \\ &\quad + \bar{s}_{\text{eq}} \exp(-k_{\text{off}} t) \end{aligned} \quad (7)$$

where $\tau_D = \sigma^2/D$. The experimental FDAP curves for 3xPAGFP and PAGFP-tub were fitted by the corresponding theoretical scenario of Eqs. 7 by the method of least squares. Fitting with the pure-diffusion scenario yields the diffusion constant, whereas fitting with the second scenario can additionally yield information about the relative free and bound fractions. The fitting was performed using a self-written Python script (van Rossum and de Boer, 1991; Oliphant, 2007). To calculate 95% confidence intervals for the estimated parameters, we used the formulas for nonlinear data fitting given in Bates and Watts (1988).

Calculation of the minimal distance between two bound tau molecules

We first calculated the average area occupied by a bound tau molecule on a single MT:

$$\langle A \rangle = \frac{S_{\text{MT}}}{N_{\text{tau}}} \quad (8)$$

where S_{MT} is the total area of the MT surfaces in the cellular process and N_{tau} is the total number of bound tau molecules in this process. Given the total concentration of tau, c_{tot} , the ratio at which it is bound on average over time, \bar{s}_{eq} , and the geometry of the cellular process as shown in Figure 2A, one can expand Eq. 8 as follows:

$$\langle A \rangle = \frac{S_{\text{MT}}}{N_{\text{tau}}} = \frac{N \cdot 2\pi R_{\text{MT}} h}{s_{\text{eq}} c_{\text{tot}} \pi R^2 h} = \frac{2R_{\text{MT}} N}{s_{\text{eq}} c_{\text{tot}} R^2} \quad (9)$$

where N is the total number of MTs in the process, R_{MT} is the radius of a single MT, R is the radius of the cellular process, and h is the length of an arbitrary process segment. Because $\langle A \rangle$ scales as l^2 , where l is the linear size of the area, one can estimate the minimal distance between two bound tau molecules by extracting the square root from $\langle A \rangle$. Substituting the numerical values for the parameters in Eq. 9, one obtains $l \approx 45 \text{ nm}$.

Other methods

Western blot analysis was performed as described elsewhere (Gauthier-Kemper *et al.*, 2011).

ACKNOWLEDGMENTS

We thank Vanessa Herkenhoff for technical help, Rainer Kurre for assistance with microscopy devices, and Christian P. Richter for providing the code for localization and tracking. W.J. holds a Niedersachsen-Professur, awarded by the state of Lower Saxony. This work was supported by the Bundesministerium für Bildung und Forschung (KMU-innovativ-7; R.B.) and the Z-project of the SFB944.

REFERENCES

- Aronov S, Aranda G, Behar L, Ginzburg I (2001). Axonal tau mRNA localization coincides with tau protein in living neuronal cells and depends on axonal targeting signal. *J Neurosci* 21, 6577–6587.
- Bakota L, Brandt R, Heinisch JJ (2012). Triple mammalian/yeast/bacterial shuttle vectors for single and combined Lentivirus-and Sindbis virus-mediated infections of neurons. *Mol Genet Genomics* 287, 313–324.
- Ballatore C, Lee VM-Y, Trojanowski JQ (2007). Tau-mediated neurodegeneration in Alzheimer's disease and related disorders. *Nat Rev Neurosci* 8, 663–672.
- Bates DM, Watts DG (1988). *Nonlinear Regression Analysis and Its Applications*, New York: Wiley.
- Brandt R, Lee G (1993a). Functional organization of microtubule-associated protein tau. Identification of regions which affect microtubule growth, nucleation, and bundle formation in vitro. *J Biol Chem* 268, 3414–3419.
- Brandt R, Lee G (1993b). The balance between tau protein's microtubule growth and nucleation activities: implications for the formation of axonal microtubules. *J Neurochem* 61, 997–1005.
- Butner KA, Kirschner MW (1991). Tau protein binds to microtubules through a flexible array of distributed weak sites. *J Cell Biol* 115, 717.
- Cleveland DW, Hwo SY, Kirschner MW (1977). Purification of tau, a microtubule-associated protein that induces assembly of microtubules from purified tubulin. *J Mol Biol* 116, 207–225.
- Dawson HN, Ferreira A, Eyster MV, Ghoshal N, Binder LI, Vitke MP (2001). Inhibition of neuronal maturation in primary hippocampal neurons from τ deficient mice. *J Cell Sci* 114, 1179–1187.
- Fath T, Eidenmüller J, Brandt R (2002). Tau-mediated cytotoxicity in a pseudohyperphosphorylation model of Alzheimer's disease. *J Neurosci* 22, 9733–9741.
- Galbraith JA, Reese TS, Schlieff ML, Gallant PE (1999). Slow transport of unpolymerized tubulin and polymerized neurofilament in the squid giant axon. *Proc Natl Acad Sci USA* 96, 11589–11594.
- Gardner MK, Charlebois BD, Jánosi IM, Howard J, Hunt AJ, Odde DJ (2011). Rapid microtubule self-assembly kinetics. *Cell* 146, 582–592.
- Gauthier-Kemper A, Weissmann C, Golovayshkina N, Sebö-Lemke Z, Drewes G, Gerke V, Heinisch JJ, Brandt R (2011). The frontotemporal dementia mutation R406W blocks tau's interaction with the membrane in an annexin A2-dependent manner. *J Cell Biol* 192, 647.
- Gauthier-Kemper A, Weissmann C, Reyher H-J, Brandt R (2012). Monitoring cytoskeletal dynamics in living neurons using fluorescence photoactivation. *Methods Enzymol* 505, 3–21.
- Hess ST, Girirajan TPK, Mason MD (2006). Ultra-high resolution imaging by fluorescence photoactivation localization microscopy. *Biophys J* 91, 4258–4272.
- Hink MA (2000). Structural dynamics of green fluorescent protein alone and fused with a single chain Fv protein. *J Biol Chem* 275, 17556–17560.
- Hinrichs MH, Jalal A, Brenner B, Mandelkow E, Kumar S, Scholz T (2012). Tau protein diffuses along the microtubule lattice. *J Biol Chem* 287, 38559–38568.
- Hirokawa N, Shiomura Y, Okabe S (1988). Tau proteins: the molecular structure and mode of binding on microtubules. *J Cell Biol* 107, 1449–1459.
- Hirokawa N, Takemura R (2005). Molecular motors and mechanisms of directional transport in neurons. *Nat Rev Neurosci* 6, 201–214.
- Hundelt M, Fath T, Selle K, Oesterwind K, Jordan J, Schultz C, Götz J, von Engelhardt J, Monyer H, Lewejohann L, et al. (2011). Altered phosphorylation but no neurodegeneration in a mouse model of tau hyperphosphorylation. *Neurobiol Aging* 32, 991–1006.
- Igaev M, Janning D, Sündermann F, Niewidok B, Brandt R, Junge W (2014). A refined reaction-diffusion model of tau-microtubule dynamics and its application in FDAP analysis. *Biophys J*, j.bj.2014.09.016.
- Irwin DJ, Lee VM-Y, Trojanowski JQ (2013). Parkinson's disease dementia: convergence of α -synuclein, tau and amyloid- β pathologies. *Nat Rev Neurosci* 14, 626–636.
- Iltner LM, Götz J (2010). Amyloid- β and tau—a toxic pas de deux in Alzheimer's disease. *Nat Rev Neurosci* 12, 67–72.
- Iltner LM, Ke YD, Delerue F, Bi M, Gladbach A, van Eersel J, Wölfling H, Chieng BC, Christie MJ, Napier IA, et al. (2010). Dendritic function of tau mediates amyloid- β toxicity in Alzheimer's disease mouse models. *Cell* 142, 387–397.
- Jacobs JR, Stevens JK (1986). Changes in the organization of the neuritic cytoskeleton during nerve growth factor-activated differentiation of PC12 cells: a serial electron microscopic study of the development and control of neurite shape. *J Cell Biol* 103, 895–906.
- Jendretzki A, Ciklic I, Rodicio R, Schmitz H-P, Heinisch JJ (2009). Cyk3 acts in actomyosin ring independent cytokinesis by recruiting Inn1 to the yeast bud neck. *Mol Genet Genomics* 282, 437–451.
- Kaether C, Skehel P, Dotti CG (2000). Axonal membrane proteins are transported in distinct carriers: a two-color video microscopy study in cultured hippocampal neurons. *Mol Biol Cell* 11, 1213–1224.
- Kempf M, Clement A, Faissner A, Lee G, Brandt R (1996). Tau binds to the distal axon early in development of polarity in a microtubule- and microfilament-dependent manner. *J Neurosci* 16, 5583–5592.
- Konzack S, Thies E, Marx A, Mandelkow EM, Mandelkow E (2007). Swimming against the tide: mobility of the microtubule-associated protein tau in neurons. *J Neurosci* 27, 9916–9927.
- Litman P, Barg J, Rindzoonski L, Ginzburg I (1993). Subcellular localization of tau mRNA in differentiating neuronal cell culture: implications for neuronal polarity. *Neuron* 10, 627–638.
- Lorberg A, Schmitz HP, Jacoby JJ, Heinisch JJ (2001). Lrg1p functions as a putative GTPase-activating protein in the Pkc1p-mediated cell integrity pathway in *Saccharomyces cerevisiae*. *Mol Genet Genomics* 266, 514–526.
- Los GV, Encell LP, McDougall MG, Hartzell DD, Karassina N, Zimprich C, Wood MG, Learish R, Ohana RF, Urh M, et al. (2008). HaloTag: a novel protein labeling technology for cell imaging and protein analysis. *ACS Chem Biol* 3, 373–382.
- Maeder CI, Hink MA, Kinkhabwala A, Mayr R, Bastiaens PIH, Knop M (2007). Spatial regulation of Fus3 MAP kinase activity through a reaction-diffusion mechanism in yeast pheromone signalling. *Nat Cell Biol* 9, 1319–1326.
- Michelman-Ribeiro A, Mazza D, Rosales T, Stasevich TJ, Boukari H, Rishi V, Vinson C, Knutson JR, McNally JG (2009). Direct measurement of association and dissociation rates of DNA binding in live cells by fluorescence correlation spectroscopy. *Biophys J* 97, 337–346.
- Morris M, Maeda S, Vossel K, Mucke L (2011). The many faces of tau. *Neuron* 70, 410–426.
- Mukrasch MD, Bibow S, Korukottu J, Jeganathan S, Biernat J, Griesinger C, Mandelkow E, Zweckstetter M (2009). Structural polymorphism of 441-residue tau at single residue resolution. *PLoS Biol* 7, e34.
- Mylonas E, Hascher A, Bernado P, Blackledge M, Mandelkow E, Svergun DI (2008). Domain conformation of tau protein studied by solution small-angle x-ray scattering. *Biochem* 47, 10345–10353.
- Newton AC (1995). Protein kinase C: structure, function, and regulation. *J Biol Chem* 270, 28495–28498.
- Oliphant TE (2007). Python for scientific computing. *Comput Sci Eng* 9, 10–20.
- Popov S, Poo MM (1992). Diffusional transport of macromolecules in developing nerve processes. *J Neurosci* 12, 77–85.
- Seeger MA, Rice SE (2010). Microtubule-associated protein-like binding of the kinesin-1 tail to microtubules. *J Biol Chem* 285, 8155–8162.
- Selkoe DJ (2013). SnapShot: pathobiology of Alzheimer's disease. *Cell* 154, 468–468.
- Sergé A, Bertaux N, Rigneault H, Marguet D (2008). Dynamic multiple-target tracing to probe spatiotemporal cartography of cell membranes. *Nat Methods* 5, 687–694.
- Spillantini MG, Goedert M (2013). Tau pathology and neurodegeneration. *Lancet Neurol* 12, 609–622.
- Sprague BL, Pego RL, Stavreva DA, McNally JG (2004). Analysis of binding reactions by fluorescence recovery after photobleaching. *Biophys J* 86, 3473–3495.
- Swaminathan R, Bicknese S, Periasamy N, Verkman AS (1996). Cytoplasmic viscosity near the cell plasma membrane: translational diffusion of a small fluorescent solute measured by total internal reflection-fluorescence photobleaching recovery. *Biophys J* 71, 1140–1151.
- Tulu US, Rusan NM, Wadsworth P (2003). Peripheral, non-centrosome-associated microtubules contribute to spindle formation in centrosome-containing cells. *Curr Biol* 13, 1894–1899.
- VandeVondele S, Vörös J, Hubbell JA (2003). RGD-grafted poly-L-lysine-graft-(polyethylene glycol) copolymers block non-specific protein adsorption while promoting cell adhesion. *Biotechnol Bioeng* 82, 784–790.
- Van Rossum G, de Boer J (1991). Interactively testing remote servers using the Python programming language. *CWI Q* 4, 283–303.
- Weimann L, Ganzinger KA, McColl J, Irvine KL, Davis SJ, Gay NJ, Bryant CE, Klenerman D (2013). A quantitative comparison of single-dye tracking analysis tools using Monte Carlo simulations. *PLoS One* 8, e64287.
- Weissmann C, Reyher HJ, Gauthier A, Steinhoff HJ, Junge W, Brandt R (2009). Microtubule binding and trapping at the tip of neurites regulate tau motion in living neurons. *Traffic* 10, 1655–1668.
- Wilmes S, Staufenbiel M, Liße D, Richter CP, Beutel O, Busch KB, Hess ST, Piehler J (2012). Triple-color super-resolution imaging of live cells: resolving submicroscopic receptor organization in the plasma membrane. *Angew Chem* 124, 4952–4955.
- Yuan A, Kumar A, Peterhoff C, Duff K, Nixon RA (2008). Axonal transport rates in vivo are unaffected by tau deletion or overexpression in mice. *J Neurosci* 28, 1682–1687.